

FROM SUPERVISION TO EXPLORATION: WHAT DOES PROTEIN LANGUAGE MODEL LEARN DURING REINFORCEMENT LEARNING?

Hanqun Cao^{1,5*} Hongrui Zhang^{2*} Junde Xu¹ Zhou Zhang⁴
 Lingdong Shen² Minghao Sun⁶ Ge Liu⁷ Jinbo Xu⁸ Wu-Jun Li⁴
 Jinren Ni² Cesar de la Fuente-Nunez⁵ Tianfan Fu⁴ Yejin Choi³
 Pheng-Ann Heng¹ Fang Wu^{3†}

¹The Chinese University of Hong Kong ²Peking University ³Stanford University

⁴Nanjing University ⁵University of Pennsylvania ⁶National University of Singapore

⁷University of Illinois Urbana-Champaign ⁸Toyota Technological Institute at Chicago

ABSTRACT

Protein Language Models (PLMs) have achieved significant breakthroughs in computational protein science through pre-training on large-scale sequence databases and leveraging scalable network architectures. Concurrently, Reinforcement Learning (RL) has demonstrated substantial progress across multiple protein design tasks by enabling expanded exploration capabilities and precise multi-objective optimization. While RL has shown transformative potential in natural language processing by enabling models to discover emergent capabilities beyond their training distributions, its capacity to unlock latent functional patterns within protein sequence space remains underexplored. In this study, we investigate whether RL-enhanced PLMs can transcend their pre-training limitations and identify implicit sequence-structure-function relationships not explicitly encoded in foundational datasets. Through systematic evaluation across four critical protein design domains—*antimicrobial peptide (AMP) design, kinase optimization, antibody engineering, and inverse folding*—we employ diverse RL algorithms and model architectures to address this fundamental question. Our comprehensive analysis demonstrates that RL reliably improves sampling efficiency across domains and, more importantly, that its effectiveness is governed by a three-factor interaction: *task difficulty, reward model accuracy, and policy capacity*. Gains scale when rewards are accurate and informative, policies have sufficient capacity to realize the signal, and tasks present headroom beyond supervised learning; conversely, noisy rewards or capacity bottlenecks cap improvements despite exploration. This principled view offers practical guidance for RL in protein design: prioritize reward refinement before scaling policy size, match RL algorithms and regularization strength to task difficulty, and allocate capacity where marginal gains are largest. Implementation is available at [github](https://github.com/fangwu/protein-rl).

1 INTRODUCTION

Protein Language Models (PLMs) have emerged as the cornerstone of computational protein design, leveraging vast training datasets and scalable network architectures to achieve remarkable success across feature representation (Lin et al., 2023; Hayes et al., 2024; Brandes et al., 2022), sequence generation (Nijkamp et al., 2023; Ferruz et al., 2022; Bhatnagar et al., 2025; Truong Jr & Bepler, 2023), and functional prediction (Su et al., 2023; Hayes et al., 2024; Xu et al., 2023a; Wu et al., 2023). These advances have successfully propelled the development of sequence-function relationship studies and protein design applications (Qiu et al., 2024; Zhang et al., 2025; Ruffolo et al., 2025).

*Equal Contribution

†Corresponding Author: fangwu@stanford.edu

However, functional protein design reveals fundamental limitations of supervised learning approaches. Traditional methods face three critical obstacles: first, the inability to optimize for complex, non-differentiable biological objectives such as TM-Score (Zhang & Skolnick, 2005) that often require iterative refinement (Yang et al., 2019); second, being constrained to interpolate within existing sequence-function mappings, thereby struggling to explore novel functional regions (Johnston et al., 2023; Notin et al., 2023); third, the inability to integrate multi-objective criteria or real-time experimental feedback (Jiang et al., 2024; Yang et al., 2025). These limitations restrict the discovery of innovative protein sequences, creating a critical gap between computational capabilities and practical engineering requirements.

Reinforcement Learning directly addresses these challenges by enabling exploration beyond observed data, supporting multi-objective optimization, and integrating expert or experimental feedback at scale. Recent studies, which are summarized in Table 4, have demonstrated the transformative potential of RL across multiple protein design tasks (Lutz et al., 2023; Xu et al., 2025; Wang et al.). When coupled with PLMs, RL gains additional power. Numerous current studies have substantiated this advantage. For instance, EvoPlay (Wang et al., 2023) discovered fluorescent proteins with several-fold higher activity than wild-type through Monte Carlo tree search exploration. ProteinZero (Wang et al., 2025b) developed proteins with enhanced designability, thermostability, and greater diversity through diversity-based Generalized Reward-based Policy Optimization (GRPO) (Shao et al., 2024). ApexAmphion (Cao et al., 2025b) successfully explored broader and more potent AMP candidates through Proximal Policy Optimization (PPO) (Schulman et al., 2017). These methods transcend the limitations of supervised training through reward-based exploration.

Simultaneously, developments in natural language processing have revealed RL’s potential for enhancing task performance and developing novel reasoning strategies (Liu et al., 2025c), though some research suggests that RL primarily amplifies existing outputs (Yue et al., 2025; Wu et al., 2025). This raises a fundamental question:

Do new emergent capabilities arise during the RL fine-tuning process of PLMs?

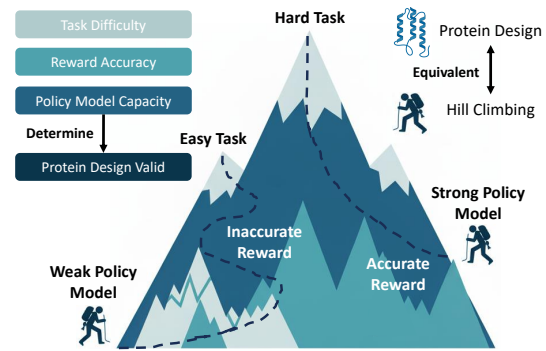


Figure 1: Reinforcement learning for protein design is akin to hill climbing. Task difficulty equates to mountain height, policy model capacity to the starting altitude, and reward accuracy to direction correctness. These three factors jointly determine the RL efficacy in protein design.

To the best of our knowledge, this study is the first to systematically evaluate this question in the context of protein design. We conduct experiments across four biological systems—*antimicrobial peptide design*, *kinase optimization*, *antibody mutation*, and *protein inverse folding*—to probe how RL interacts with PLMs. Our results show that RL consistently improves sampling efficiency for beneficial sequences. More importantly, we find that RL’s effectiveness is determined by the interaction of three key factors: *task difficulty*, defined by the ruggedness and observability of the underlying fitness landscape; *reward model accuracy*, reflecting how well the reward signal is calibrated and how much signal-to-noise it conveys; and *policy model capacity*, which depends on model size, representational power, and initialization quality. As shown in Fig. 1, RL training for protein design can be likened to hill-climbing: task difficulty sets the height of the summit to be scaled, reward accuracy determines the climbing direction, and policy-model capacity fixes the starting altitude. These factors jointly shape whether RL can climb towards subspaces with stronger task alignment or stall in suboptimal plateaus. Different combinations of task complexity, reward fidelity, and policy strength yield qualitatively distinct trajectories of improvement. We believe this framework provides a principled way to measure current RL–PLM systems and serves as a practical blueprint for guiding future RL applications in protein design.

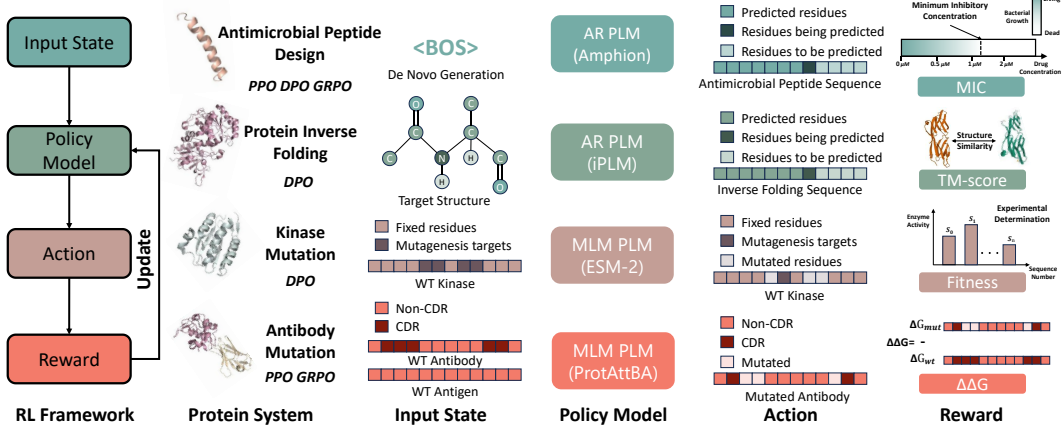


Figure 2: **Overview of the four biological systems** based on PLM and RL. **AR** and **MLM** denote Auto-regressive and Masked Language Modeling, respectively.

2 METHOD

Notations. We define a unified framework for protein sequence optimization tasks. Let $\mathcal{A} = \{A, C, D, E, F, G, H, I, K, L, M, N, P, Q, R, S, T, V, W, Y\}$ denote the set of 20 natural amino acids, which compose the vocabulary of protein design, and $\mathcal{S} = \mathcal{A}^*$ represent the space of all finite protein sequences.

2.1 PROTEIN INVERSE FOLDING

For protein inverse folding, we address structure-to-sequence mapping where the policy model $\pi_\theta(\mathbf{s}|\mathbf{z})$ generates sequences conditioned on target 3D structure $\mathbf{z} \in \mathcal{Z}$ (Xu et al., 2025). The optimization objective combines sequence likelihood with designability constraints:

$$\mathbf{s}^* = \arg \max_{\mathbf{s} \in \mathcal{S}} \mathbb{E}_{\mathbf{s} \sim \pi_\theta(\cdot|\mathbf{z})} [\log p(\mathbf{s}|\mathbf{z}) + \lambda \Xi(\mathbf{s}, \mathbf{z})], \quad (1)$$

where $p(\mathbf{s}|\mathbf{z})$ represents the structure-conditioned sequence probability and $\Xi(\mathbf{s}, \mathbf{z})$ captures designability constraints that ensure the generated sequence can fold into the target structure.

We employ InstructPLM-7B (Qiu et al., 2024) as our policy model, initially trained on the CATH 4.2 dataset (Sillitoe et al., 2021) to establish inverse folding capabilities. The action space corresponds to autoregressive sequence generation, where at each step t , the policy selects amino acid token $a_t \in \mathcal{A}$ according to:

$$a_t \sim \pi_\theta(a_t|\mathbf{z}, a_{1:t-1}), \quad (2)$$

where \mathbf{z} represents the target structure and $a_{1:t-1}$ denotes previously generated tokens. The complete sequence is constructed through iterative token selection until reaching the end-of-sequence token.

We applied TM-Score as the reward function for structural fidelity evaluation. By employing ESM-Fold (Lin et al., 2023) to predict the structure \mathbf{z}_{pred} for each generated sequence, we calculate the TM-Score as $\text{TM-Align}(\mathbf{z}, \mathbf{z}_{pred})$ (Zhang & Skolnick, 2005).

We then implement Direct Preference Optimization (DPO) (Ferruz et al., 2024) enhanced with regularization. For each target structure, we sample sequences using the current policy model, evaluate the TM-Scores, and rank them to create preference pairs with high-scoring sequences as positive examples S_w and low-scoring sequences as negative examples S_l . The loss function combines standard DPO with supervised regularization (Xue et al., 2025):

$$\mathcal{L}(\pi_\theta, \pi_{ref}) = -\mathbb{E}_{(\mathbf{z}, S_w, S_l) \sim D_{pair}} \left[\underbrace{\log \sigma \left(\beta \log \frac{\pi_\theta(S_w|\mathbf{z})}{\pi_{ref}(S_w|\mathbf{z})} - \beta \log \frac{\pi_\theta(S_l|\mathbf{z})}{\pi_{ref}(S_l|\mathbf{z})} \right)}_{\mathcal{L}_{DPO}} - \underbrace{\lambda \log(\pi_\theta(S_w|\mathbf{z}))}_{\mathcal{L}_{reg}} \right], \quad (3)$$

where \mathcal{L}_{reg} maintains sequence fidelity by encouraging the model to assign high probability to structurally superior sequences. We employ multi-round iterative refinement, where each round generates updated preference data and refreshes reference weights for progressive improvement.

2.2 ANTIMICROBIAL PEPTIDE DESIGN

For AMP design, we generate peptides with enhanced antimicrobial activity by targeting lower MIC (minimum inhibitory concentration) values, indicating stronger bacterial inhibition. We employ Amphion-SFT (Cao et al., 2025b), an autoregressive PLM trained on AMPs, as our policy model $\pi_\theta(\mathbf{s})$ to generate sequences optimized for antimicrobial potency. The optimization objective is:

$$\mathbf{s}^* = \arg \max_{\mathbf{s} \in \mathcal{S}_{AMP}} \mathbb{E}_{\mathbf{s} \sim \pi_\theta} [f_{MIC}(\mathbf{s})], \quad (4)$$

where $f_{MIC} : \mathcal{S}_{AMP} \rightarrow \mathbb{R}$ denotes ApexMIC (Cao et al., 2025b), a binary classifier for predicting antimicrobial potential. The reward function transforms the predicted score through normalization:

$$R(\mathbf{s}) = 2 \cdot (f_{MIC}(\mathbf{s}) - \lambda), \quad (5)$$

where $\lambda = 0.4$ denotes the threshold for binary classification, providing balanced reward estimation.

We implement DPO (Ferruz et al., 2024), PPO (Schulman et al., 2017), and GRPO (Shao et al., 2024) for fine-tuning. An additional KL regularization term is added in the loss of PPO and GRPO to keep the naturalness of generated AMPs. Detailed formulations are shown in Appendix C.4.

2.3 KINASE MUTATION

The kinase mutation task requires the model to perform multi-step mutations at specified positions of the initial sequence, where each step involves selecting both the mutation site and the amino acid substitution to progressively enhance the final mutant’s fitness. Consider a wild-type protein sequence $\mathbf{s}_0 = (s_{0,1}, s_{0,2}, \dots, s_{0,n}) \in \mathcal{S}$ where $s_{0,i} \in \mathcal{A}$. The fitness optimization objective is:

$$\mathbf{s}^* = \arg \max_{\mathbf{s}' \in \mathcal{S}} \Phi(\mathbf{s}'), \quad (6)$$

where $\Phi : \mathcal{S} \rightarrow \mathbb{R}$ quantifies protein fitness.

We adopt the ESM-2 architecture as our base model and follow the training framework described in Wang et al. (2024). The annotated fitness value serves as the reward, and the policy model performs multi-step mutations on the wild-type sequence s_0 to maximize fitness of the final sequence s_t . The action space consists of position selection and amino-acid selection defined as $a_t = (\hat{p}_t, \hat{x}_t)$ where $\hat{x}_t \neq s_{t-1}[\hat{p}_t]$. The policy model uses ESM2 embeddings and MLP to predict mutation position, then replaces the corresponding residue with [MASK] token and employs ESM-2 to select the new amino acid. During DPO training, we did not employ either the KL penalty or the entropy regularization term (See details in Section C.4).

2.4 ANTIBODY OPTIMIZATION

For antibody optimization, we consider the complex space $\mathcal{C} = \mathcal{S}_{ab} \times \mathcal{S}_{ag}$ where \mathcal{S}_{ab} and \mathcal{S}_{ag} represent antibody and antigen sequence spaces. Given a fixed antigen sequence \mathbf{s}_{ag} , the policy model $p_\theta(\mathbf{s}_{ab}|\mathbf{s}_{ag})$ aims to generate optimized antibody sequences that minimize binding affinity change:

$$\mathbf{s}_{ab}^* = \arg \min_{\mathbf{s}_{ab}} \mathbb{E}_{\mathbf{s}_{ab} \sim p_\theta(\cdot|\mathbf{s}_{ag})} [\Delta\Delta G(\mathbf{s}_{ab}, \mathbf{s}_{ag})], \quad (7)$$

where $\Delta\Delta G(s_{ab}, s_{ag}) = \Psi(\mathbf{s}_{ab}, \mathbf{s}_{ag}) - \Psi(\mathbf{s}_{ab}^{wt}, \mathbf{s}_{ag})$ denotes the binding affinity change from wild-type, which is predicted by a re-implemented version of ProtAttBA (Liu et al., 2025a). The new architecture is designed to better model the action of the policy model through logits (See details in Alg.1). Instead of training by regression on $\Delta\Delta G$ (Liu et al., 2025a), we re-designed its training loss with combined objectives:

$$\mathcal{L}_{total} = \mathcal{L}_{reg} + \lambda \mathcal{L}_{MLM}, \quad (8)$$

where \mathcal{L}_{reg} represents the original $\Delta\Delta G$ regression loss and \mathcal{L}_{MLM} denotes masked language modeling (MLM) loss. We achieved higher performance on the test set (Tab. D.1).

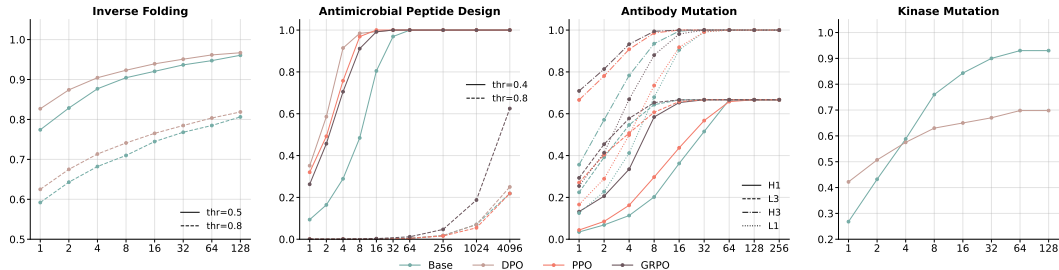


Figure 3: Pass@k results for four biological systems.

The wild-type antibody sequence is mutated through policy logits $\mathbf{z} \in \mathbb{R}^{L \times |\mathcal{A}|}$ where L denotes sequence length, combined with a position head that selects mutation sites within CDR. Mutated sequences are generated through multinomial sampling from the policy logits of antibody at selected CDRs, with detailed procedures described in Algorithm 2. We employ rollout mechanisms and compute Generalized Advantage Estimation (GAE), with a value model initialized using an MLP architecture.

We applied both PPO and GRPO for model training. The comprehensive loss function is as follows:

$$\mathcal{L}_{total} = \mathcal{L}_{policy} + \alpha \mathcal{L}_{KL} + \beta \mathcal{L}_{value} + \gamma \mathcal{L}_{entropy}, \quad (9)$$

where \mathcal{L}_{policy} denotes the standard policy loss for PPO and GRPO (See details in Appendix C.4), \mathcal{L}_{KL} denotes the clamped KL divergence loss between current and reference policies, \mathcal{L}_{value} denotes the regression loss for value function, and $\mathcal{L}_{entropy}$ represents position entropy computed over mutation position logits to encourage exploration. The coefficients α , β , and γ balance the contribution of each component.

3 EXPERIMENTS

3.1 DATASETS AND EVALUATION METRICS

Datasets The kinase mutation experiments utilize PhoQ (Podgornaia & Laub, 2015) containing 140,517 annotated variants from 160,000 (20^4) possible mutations at four sites (A284, V285, S288, T289), with unlabeled variants assigned fitness values of -1. The antibody mutation task employs the AB1101 dataset (Wang et al., 2020) comprising 32 antigen-antibody complexes with 645 single-point mutations for training and 456 multi-point mutations for testing, where complexes 1MLC and 1VFB serve as designated test structures. RL design leverages sequences from DBAASP, DRAMP, and APD3 databases Pirtskhala et al. (2021); Shi et al. (2022); Wang et al. (2016), yielding 7,888 samples (peptides 6-50 amino acids, active threshold $<32 \mu\text{M}/\text{mL}$ MIC) split via MMseqs2 (Steinegger & Söding, 2017) clustering into 6,153 training, 789 validation, and 946 test samples. Protein inverse folding experiments use CATH4.2 (Sillitoe et al., 2021) with 18,024 training structures for base model and DPO training, evaluated on the CATH4.2 test set (1,120 structures) combined with TS50 (50 structures) and TS500 (470 structures) benchmarks.

Evaluation Metric Pass@k metric is applied to evaluate model’s sampling efficiency for objective-satisfying feasible sequences, which is calculated by the probability of succeeding at least once by taking the complement of the probability of failing in all k consecutive trials. It is formally defined as:

$$\text{Pass}@k(p) = 1 - (\Pr_{y \sim p(y|x)}[R(x, y) = 0])^k, \quad (10)$$

where $p(y|x)$ is the output probability distribution of the model for a given prompt x . $R(x, y)$ is a reward function that returns 1 if the completion y is correct, and 0 otherwise. The term $\Pr_{y \sim p(y|x)}[R(x, y) = 0]$ denotes the probability of an incorrect answer in a single sample.

To analyze the deviation of pre- and post-RL models, we follow (Wu et al., 2025)’s definition of **Support** as a more detailed metric for pass@k. We leverage three key concepts under pass@k setting. *Shrinkage(k)* represents the set of problems that the base model could solve but the fine-tuned model cannot solve at pass@k. *Expansion(k)* denotes the set of problems that the base model

could not solve but the fine-tuned model can now solve at pass@k. *Preservation(k)* refers to the set of problems that both models can solve at pass@k. To quantify the trade-off between discovering new correct solutions and forgetting previously known ones, we propose the *Expansion-Shrinkage Ratio (ESR)*, a simple yet effective metric that captures the balance between knowledge gain and loss during fine-tuning:

$$\text{ESR}(k) = |\text{Expansion}(k)|/|\text{Shrinkage}(k)|. \quad (11)$$

An ESR greater than 1.0 indicates net knowledge gain, while an ESR less than 1.0 signals net knowledge loss, and an ESR equal to 1.0 represents balanced learning dynamics.

Table 1: Results for *Support* metric for four biological systems.

	Preservation	Expansion	Shrinkage	Out-of-support	ESR \uparrow
AMP design	290	7	49	4	0.14
Kinase mutation	260	8	100	32	0.08
Antibody mutation	8	2	4	2	0.50
Inverse folding	891	9	21	199	2.33

Biological Metrics. We applied multiple metrics to evaluate the biological reasonability. (i) *Positional entropy* is applied to evaluate sequence diversity at individual positions within the complementarity-determining regions of both kinase and antibody mutation tasks, measuring the uncertainty across mutational sites. (ii) *Perplexity* is applied to evaluate the likelihood quality of generated protein sequences across all tasks, computed as the exponential of the average negative log-likelihood under the respective models. (iii) *Diversity and Novelty* are applied to evaluate sequence variation and distinctiveness within generated outputs for both RL design and protein inverse folding tasks, calculated as average sequence similarity between generated sequences and the average of one minus maximum sequence similarity scores, respectively. (iv) *Recovery rate* and *TM-score* are applied to evaluate sequence similarity and structure similarity in protein inverse folding tasks.

3.2 INVERSE FOLDING

In the inverse folding task, RL fine-tuned the base model, resulting in higher TM-scores, as demonstrated by the improved pass@k performance and TM-score distribution (Figure 4C). Across all values of k and both thresholds (0.5 and 0.8), the RL model consistently outperformed the base model, indicating more effective exploration toward higher-quality structural predictions. This suggests that RL learned to focus on sequence–structure relationships that maximize TM-scores.

The RL model showed lower perplexity in the DPO variant (Figure 4B), indicating that it sampled more efficiently compared to the base model. However, as shown in Figure 4A, the RL model exhibited slightly reduced novelty and diversity but higher recovery, suggesting that RL exploration prioritized regions with high TM-scores, at the cost of reduced exploration in diverse regions.

When stricter evaluation criteria were applied (TM-score > 0.8 and sequence similarity < 0.7), expansion cases outnumbered shrinkage cases across all k-values, demonstrating that RL exploration expanded the design space (Figure 7). Smaller k-values, however, resulted in decreased ESR, suggesting that RL’s sampling efficiency is more pronounced at larger k-values.

UMAP visualization (Figure 4D) further supports this conclusion, showing that the RL model’s sampling distribution aligns with a subset of the base model’s, with distinct expansion and shrinkage regions. This indicates that RL’s exploration is focused on high-quality structural solutions while maintaining a core subset of diverse sequences.

In the inverse folding task, RL fine-tuned the base model, effectively navigating the task’s moderate complexity and rugged landscape. This allowed the model to prioritize high-quality structural solutions, as indicated by the improved TM-scores and pass@k performance (Figure 4C). The RL model’s reduced perplexity (Figure 4B) suggests more efficient sampling, with exploration directed toward high-reward regions characterized by better structural similarity. However, this focus on high-reward regions came at the cost of diversity and novelty, as seen in the slightly reduced values for these metrics (Figure 4A).

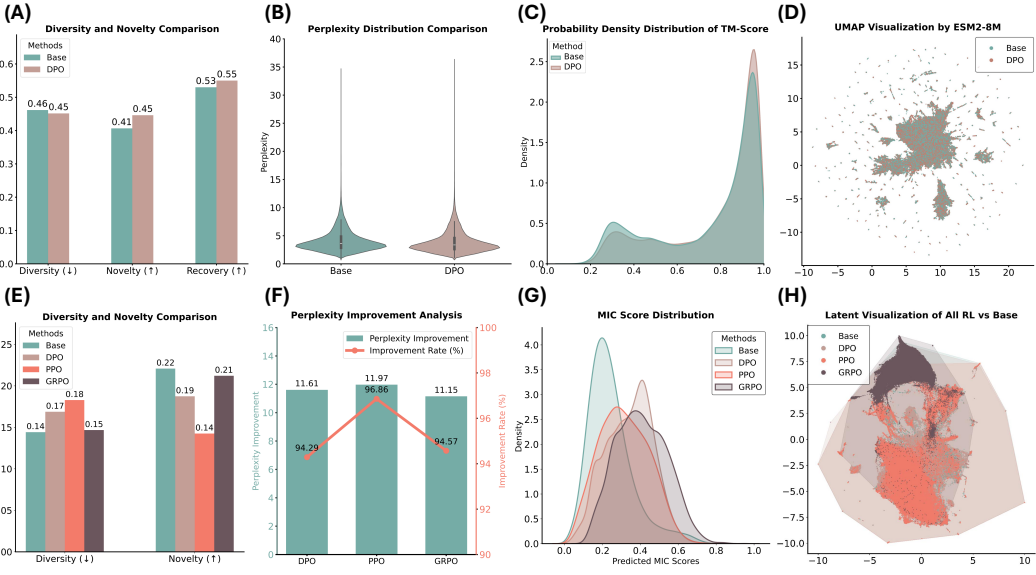


Figure 4: Experimental results for inverse folding (A-D) and AMP design (E-H).

3.3 ANTIMICROBIAL PEPTIDE DESIGN

In the AMP design task, RL fine-tuned the base model to generate AMPs with lower MIC values. As shown in Figure 4F, the RL model outperformed the base model, with approximately 95% of the generated samples achieving lower perplexity, indicating more efficient sampling. This suggests that RL effectively directed exploration toward high-reward regions associated with lower MIC values.

In the pass@k evaluation (Figure 3), all RL models (DPO, PPO, and GRPO) outperformed the base model, particularly under the challenging 0.8 threshold for binary classification. While DPO and PPO performed similarly to the base model, GRPO showed continuous improvement, reflecting its superior exploration ability. This performance boost can be attributed to GRPO's group loss mechanism, which emphasizes high-reward samples and encourages more focused exploration.

Next, we assessed sampling efficiency by constructing support sets with a cross-entropy threshold < 3.0 (Figure 4G). RL methods discarded more positive samples (ESR = 0.14) but achieved higher sampling efficiency, demonstrating a more targeted exploration approach. UMAP visualization of latent distributions further confirmed these findings: RL models, especially GRPO, concentrated within a high-reward subset of the AMP space. GRPO's distribution showed a clear shift within the base model's convex hull, indicating that it learned to focus on promising regions while maintaining coverage across the original design space. In contrast, DPO and PPO models showed reduced diversity and novelty, emphasizing GRPO's superior exploration capability.

The AMP design task involves navigating a rugged and complex search space, where low MIC values are rare (Figure 3B). RL successfully focused exploration on regions associated with lower MIC values, demonstrating its ability to tackle challenging tasks with a well-structured reward signal. The reward model's accuracy, as reflected in Table F.1, shows that RL effectively exploited the reward signal. GRPO, in particular, highlighted the significance of policy model capacity, outperforming DPO and PPO by achieving stronger exploration and prioritizing high-reward regions while maintaining coverage within the original search space.

3.4 KINASE MUTATION

In the kinase mutation task, RL fine-tuned the base model by prioritizing high-fitness sequences, at the cost of overall sequence diversity. This shift reflects the optimization objective's focus on maximizing fitness within a rugged, discontinuous protein landscape. Sampling 50,000 sequences revealed minimal overlap (76 sequences, 4%) between the base and RL models. Notably, entropy

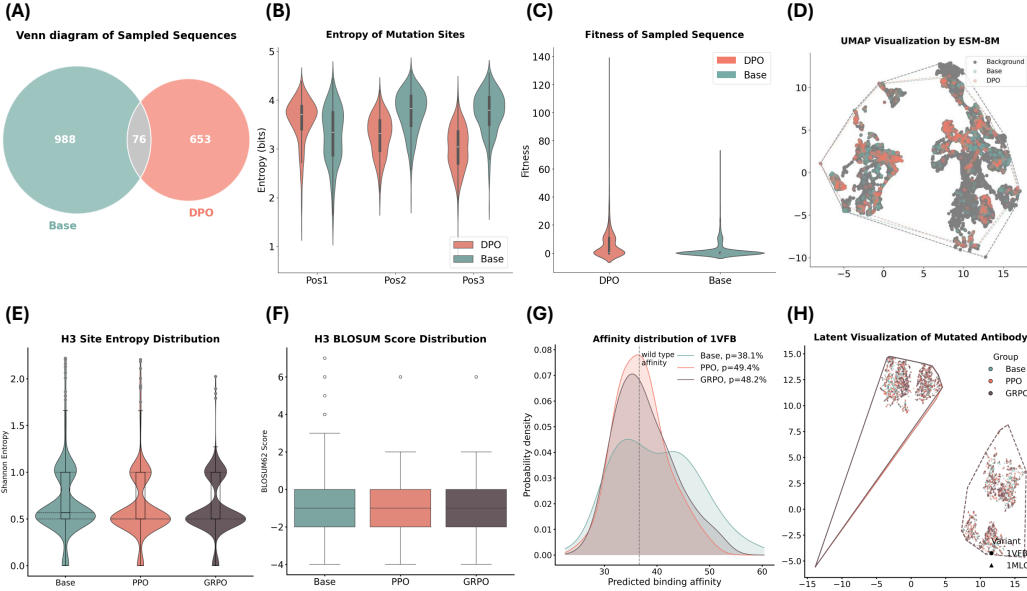


Figure 5: Experimental results for kinase mutation (A-D) and antibody optimization (E-H).

at mutable positions shifted: the RL model showed a decrease at position 1 and marked increases at positions 2 and 3, indicating a fundamental distributional shift (Figure 5A-B).

The RL model achieved a significantly higher mean fitness, with peak scores reaching 133, compared to 70 for the base model. However, the base model maintained superiority in low-fitness regions (<1), as shown in Figure 5C. Pass@k evaluation (Figure 3) confirmed this trend: RL excelled at $k=1-2$ but was overtaken by $k=4$, with the base model leading at saturation ($k=128$). When we assessed support sets at $k=32$, starting with 400 wild-type sequences from the test set, the results revealed that RL led to a contraction of the sequence space, with an ESR of only 0.08. This indicates that RL training in the kinase mutation task sacrifices some exploration capacity to focus on high-fitness regions, leading to better performance within these areas.

UMAP visualization (Figure 5D) further corroborates this finding. The RL model's sampling distribution was more concentrated compared to the base model, indicating a shift in probability mass toward high-fitness regions. While most RL sequences formed a subset of the base model's distribution, a few escaped the original convex hull, suggesting some degree of novel exploration. However, the overall RL distribution largely resembled a subset of the base model, with limited exploration outside of the original distribution.

Overall, RL effectively optimized for high-fitness regions but faced challenges in balancing exploration and exploitation due to the task's complex and discontinuous fitness landscape. The verified reward model enabled RL to focus on high-reward regions, as reflected in higher mean fitness and lower perplexity, directing sampling towards high-fitness areas. However, due to a weaker policy model (as seen in pass@k), RL's exploration efficiency was limited (ESR = 0.08). While the RL model outperformed in high-fitness regions, its limited diversity indicates that the task requires a stronger policy model to further enhance exploration.

3.5 ANTIBODY MUTATION

In the antibody mutation task, RL models fine-tuned on different CDRs (L1, L3, H1, H3) generally achieved higher pass@k values, with GRPO outperforming PPO (Figure 3). Pass@k reached 1.0 for H3 and L1 sites, while H1 and L3 tasks proved more challenging, with convergence to 0.67. These results suggest that RL effectively optimized the sampling in more accessible regions but faced difficulties in challenging tasks. Support evaluation on the test set, based on the average cross-entropy of L3 CDR sites, confirmed that RL models demonstrated higher sampling efficiency (Figure 5G). However, in some cases, shrinkage exceeded expansion (ESR = 0.5), indicating net

knowledge loss during RL training. This suggests that while RL can improve efficiency, it may also limit diversity when the exploration is overly concentrated on specific regions (Table 3.1).

Further analysis of mutated sites revealed that RL models, particularly PPO and GRPO, generated mutations with lower entropy values, while maintaining BLOSUM substitution score distributions similar to the base model (Figure 5E-F). This suggests that RL models learned to prefer more conservative mutation strategies, adhering to physicochemical constraints while optimizing for specific amino acid substitutions.

In terms of the reward function, RL models shifted towards lower ddG values, indicating a preference for more favorable energy states. The distribution of ddG values showed that RL explored regions with significantly lower ddG (Figure 6). To validate these findings and exclude potential reward-hacking artifacts, we compared the results with Protenix-Mini (Gong et al., 2025) for structural prediction of 1VFB H3 variants and FoldX (Schymkowitz et al., 2005) for affinity prediction (Figure 5G). RL models showed consistent improvements on this independent affinity function, with more concentrated distributions, despite a reduced proportion of low-energy samples.

Furthermore, analysis of reward function ddG distributions showed that RL models shifted toward lower ddG values and explored regions with substantially lower ddG (Figure 6). To exclude reward-hacking artifacts from the imperfect reward model (Spearman correlation = 0.47), we validated results using Protenix-Mini (Gong et al., 2025) for structural prediction of 1VFB H3 variants and FoldX (Schymkowitz et al., 2005) for affinity prediction (Figure 5G). RL models demonstrated consistent improvements on this independent affinity function, with more concentrated distributions despite reduced low-energy sample proportions. Visualization of two test set PDB variants showed no significant convex hull boundary shifts after RL (Figure 5H).

The antibody-antigen mutation task presents a more complex landscape, with certain CDR regions being more easily optimized than others. RL effectively optimized these more accessible regions, but the limited success in H1 and L3 tasks highlights challenges in exploring more difficult areas. These challenges stem from the relatively low accuracy of the reward model (Spearman = 0.47) and suboptimal policy model initialization (as evidenced by pass@k results). While RL prioritized exploration of energetically favorable regions, this also led to a trade-off in diversity and shrinkage (ESR = 0.5). Compared to other tasks, the antibody domain presents significantly greater challenges, requiring more valuable work to enhance the model’s exploration capability and generalizability.

4 RELATED WORKS

Protein Language Models and Beyond The landscape of protein language models compose distinct architectures: BERT-based encoder models like ESM-2 (Lin et al., 2023) excel at understanding tasks through bidirectional context, autoregressive models such as ProGen2 (Nijkamp et al., 2023) and ProtGPT2 (Ferruz et al., 2022) focus on generation, while recent approaches like ESM-3 (Hayes et al., 2024), SaProt (Su et al., 2023), and xTrimoPGLM (Chen et al., 2024) integrate multimodal information. A critical limitation of these foundational models is their general focus, which delivers diminishing returns for specialized protein tasks despite requiring substantial computational resources. This has driven emergence of protein-specific architectures, including antibody models like HTP (Wu & Li, 2023), IgLM (Shuai et al., 2023), and AbLang (Olsen et al., 2022), enzyme systems like ZymCTRL (Munsamy et al., 2024), and domain-targeted approaches for inverse folding (Qiu et al., 2024), RL design (Cao et al., 2025b) and membrane proteins (Zhang et al., 2024d). These specialized models outperform general approaches through domain-specific training, but they face fundamental limitations in terms of training data (Tang et al., 2024).

RL for Natural Language Processing Math reasoning is a key RL success in NLP, showing emergent self-verification and adaptive scaling via GRPO and RL with Verifiable Rewards (DeepSeek-AI, 2025; Zhang et al., 2024b; Cobbe et al., 2021; Xiao et al., 2025). Multimodal tasks use RL for cross-modal reasoning; MAYE and RLHF-V help vision-language models solve math and reduce hallucinations (Wu et al., 2024; Liu et al., 2024). RL is also used for compiler feedback (Zhang et al., 2024a), conversational optimization (Zhang et al., 2024c), and ranking (Paulus et al., 2017; Ranzato et al., 2015). The effectiveness of RLVR for reasoning is contested: some view it as smart sampling toward high-reward outputs (Gandhi et al., 2025; Shah et al., 2025); several studies attribute reasoning to pretraining (Yue et al., 2025; Wu et al., 2025; Wu & Choi) and argue RLVR echoes pretrained

patterns (Zhao et al., 2025). Others report gains from structured RLVR (Liu et al., 2025c) and from unlikeliness rewards to reduce rank bias (He et al., 2025). Wen et al. (2025) propose CoT-passk, showing RLVR benefits under more robust evaluation.

RL for Protein Design Current RL approaches for protein design focus on five major tasks. For **structural design** tasks, MCTS-based approaches dominate due to their ability to handle complex architectural constraints. Lutz et al. (Lutz et al., 2023) and GAPN (Gao et al., 2024) designed multimer protein complex assembly with MCTS and PPO, respectively. **Sequence optimization** represents the most diverse application area, employing various algorithms depending on multiple optimization objectives. MCTS-based methods include EvoPlay (Wang et al., 2023) for enzyme design and RelaVDEP (Mi et al., 2025) for multi-objective protein engineering. PPO-based approaches encompass RLXF (Blalock et al., 2025) for experimental feedback integration, μ Protein (Sun et al., 2025) for landscape model-guided design, and ApexAmphion (Cao et al., 2025b) for antimicrobial peptide optimization. For **inverse folding**, recent work has gravitated toward DPO and its variants, including multi-round DPO (Xu et al., 2025), EnerBridge-DPO (Rong et al., 2025), and ResiDPO (Xue et al., 2025). Alternative approaches include ProteinZero using PPO/GRPO (Wang et al., 2025b) and ProtInvTree employing MCTS (Liu et al., 2025b). **Antibody engineering** applications utilize diverse RL paradigms: AB-Gen (Xu et al., 2023b) with REINVENT for CDRH3 libraries, BetterBodies (Vogt et al., 2024) and structured Q-learning (Cowen-Rivers et al., 2022) for Q-learning-based optimization, and stability-focused approaches using reward fine-tuning (Wang et al.) and PPO (Cao et al., 2025a). Finally, **peptide binder design** employs specialized algorithms: TCRPPO (Chen et al., 2023) for T-cell receptor sequences, and MCTS-based methods like High-Play (Lin et al., 2025) and CYC_BUILDER (Wang et al., 2025a) for cyclic peptide optimization.

5 CONCLUSION

This study is the first to directly explore what reinforcement learning (RL) can teach protein language models (PLMs) in protein design tasks. Through an analysis of two leading PLM architectures, three RL algorithms, and four prominent experimental systems, we conclude that RL enables more efficient sampling of high-reward regions. However, RL’s ability to learn new patterns and optimize high-reward distributions comes with trade-offs, including reduced diversity, increased shrinkage ($ESR < 1$), and other costs. These effects are influenced by factors such as the initialization capacity of the policy model (base model), reward accuracy, and task complexity. We believe this insight offers a meaningful explanation for the current landscape of RL-based protein design. Building on this, researchers can adopt a fresh perspective on how to make RL fine-tuning more effective. While this work primarily focuses on PLMs for protein sequence design, future research will extend to Diffusion/Flow Matching architectures, protein structure and sequence-structure co-design, and additional RL algorithms (e.g., MCTS). We anticipate that the findings from this study, coupled with future validation, will provide valuable insights that drive innovation in the field.

REFERENCES

Aadyot Bhatnagar, Sarthak Jain, Joel Beazer, Samuel C Curran, Alexander M Hoffnagle, Kyle Ching, Michael Martyn, Stephen Nayfach, Jeffrey A Ruffolo, and Ali Madani. Scaling unlocks broader generation and deeper functional understanding of proteins. *bioRxiv*, pp. 2025–04, 2025.

Nathaniel Blalock, Srinath Seshadri, Agrim Babbar, Sarah A Fahlberg, Ameya Kulkarni, and Philip A Romero. Functional alignment of protein language models via reinforcement learning. *bioRxiv*, pp. 2025–05, 2025.

Nadav Brandes, Dan Ofer, Yam Peleg, Nadav Rapoport, and Michal Linial. Proteinibert: a universal deep-learning model of protein sequence and function. *Bioinformatics*, 38(8):2102–2110, 2022.

Hanqun Cao, Haosen Shi, Chenyu Wang, Sinno Jialin Pan, and Pheng-Ann Heng. Glid²e: A gradient-free lightweight fine-tune approach for discrete sequence design. In *ICLR 2025 Workshop on Generative and Experimental Perspectives for Biomolecular Design*, 2025a.

Hanqun Cao, Marcelo D. T. Torres, Jingjie Zhang, Zijun Gao, Fang Wu, Chunbin Gu, Jure Leskovec, Yejin Choi, Cesar de la Fuente-Nunez, Guangyong Chen, and Pheng-Ann Heng. A deep re-

inforcement learning platform for antibiotic discovery, 2025b. URL <https://arxiv.org/abs/2509.18153>.

Bo Chen, Xingyi Cheng, Pan Li, Yangli-ao Yang, Bin Chen, Tangkai Xu, Zhuoming Yi, Duanyang Xu, Yinghui Zheng, Qiwei Li, et al. xtrimopglm: Unified 100b-scale pre-trained transformer for deciphering the language of protein, 2024.

Ziqi Chen, Martin Renqiang Min, Hongyu Guo, Chao Cheng, Trevor Clancy, and Xia Ning. T-cell receptor optimization with reinforcement learning and mutation polices for precision immunotherapy. In *International Conference on Research in Computational Molecular Biology*, pp. 174–191. Springer, 2023.

Karl Cobbe, Vineet Kosaraju, Mohammad Bavarian, Mark Chen, Heewoo Jun, Lukasz Kaiser, Matthias Plappert, Jerry Tworek, Jacob Hilton, Reiichiro Nakano, et al. Training verifiers to solve math word problems. *arXiv preprint arXiv:2110.14168*, 2021.

Alexander I Cowen-Rivers, Philip John Gorinski, Aivar Sootla, Asif Khan, Liu Furui, Jun Wang, Jan Peters, and Haitham Bou Ammar. Structured q-learning for antibody design. *arXiv preprint arXiv:2209.04698*, 2022.

DeepSeek-AI. Deepseek-r1: Incentivizing reasoning capability in llms via reinforcement learning, 2025. URL <https://arxiv.org/abs/2501.12948>.

Yasha Ektefaie, Olivia Viessmann, Siddharth Narayanan, Drew Dresser, J Mark Kim, and Armen Mkrtchyan. Reinforcement learning on structure-conditioned categorical diffusion for protein inverse folding. *arXiv preprint arXiv:2410.17173*, 2024.

Noelia Ferruz, Steffen Schmidt, and Birte Höcker. Protgpt2 is a deep unsupervised language model for protein design. *Nature Communications*, 13(1):4348, 2022. doi: 10.1038/s41467-022-32007-7.

Noelia Ferruz, Michael Heinzinger, Mehmet Akdel, Alexander Goncearenco, Luca Naef, and Christian Dallago. Direct preference optimization of protein language models, 2024.

Kanishk Gandhi, Ayush Chakravarthy, Anikait Singh, Nathan Lile, and Noah D Goodman. Cognitive behaviors that enable self-improving reasoners, or, four habits of highly effective stars. *arXiv preprint arXiv:2503.01307*, 2025.

Ziqi Gao, Tao Feng, Jiaxuan You, Chenyi Zi, Yan Zhou, Chen Zhang, and Jia Li. Deep reinforcement learning for modelling protein complexes. *arXiv preprint arXiv:2405.02299*, 2024.

Chengyue Gong, Xinshi Chen, Yuxuan Zhang, Yuxuan Song, Hao Zhou, and Wenzhi Xiao. Proteinix-mini: Efficient structure predictor via compact architecture, few-step diffusion and switchable plm. *arXiv preprint arXiv:2507.11839*, 2025.

Tom Hayes, Rohith Krishnan, Mahdi Hashemi, Daniel Erwin, Lukas Adesina, Jeffrey Ruffolo, Nikhil Naik, and Ali Madani. Simulating 500 million years of evolution with a language model. *Science*, 386(6724):ead9496, 2024. doi: 10.1126/science.ado9496.

Andre He, Daniel Fried, and Sean Welleck. Rewarding the unlikely: Lifting gro beyond distribution sharpening. *arXiv preprint arXiv:2506.02355*, 2025.

Kaiyi Jiang, Zhaoqing Yan, Matteo Di Bernardo, Samantha R Sgrizzi, Lukas Villiger, Alisan Kayabolen, BJ Kim, Josephine K Carscadden, Masahiro Hiraizumi, Hiroshi Nishimasu, et al. Rapid in silico directed evolution by a protein language model with evolvepro. *Science*, 387(6732):eadr6006, 2024.

Kadina E Johnston, Clara Fannjiang, Bruce J Wittmann, Brian L Hie, Kevin K Yang, and Zachary Wu. Machine learning for protein engineering. In *Machine Learning in Molecular Sciences*, pp. 277–311. Springer, 2023.

Huitian Lin, Cheng Zhu, Tianfeng Shang, Ning Zhu, Kang Lin, Chengyun Zhang, Xiang Shao, Xudong Wang, and Hongliang Duan. Highplay: Cyclic peptide sequence design based on reinforcement learning and protein structure prediction. *Journal of Medicinal Chemistry*, 2025.

Zeming Lin, Halil Akin, Roshan Rao, Brian Hie, Zhongkai Zhu, Wenting Lu, Nikita Smetanin, Robert Verkuil, Ori Kabeli, Yaniv Shmueli, et al. Evolutionary-scale prediction of atomic-level protein structure with a language model. *Science*, 379(6637):1123–1130, 2023. doi: 10.1126/science.ade2574.

Chen Liu, Mingchen Li, Yang Tan, Wenrui Gou, Guisheng Fan, and Bingxin Zhou. Sequence-only prediction of binding affinity changes: a robust and interpretable model for antibody engineering. *Bioinformatics*, 41(8):btaf446, 08 2025a. ISSN 1367-4811. doi: 10.1093/bioinformatics/btaf446. URL <https://doi.org/10.1093/bioinformatics/btaf446>.

Mengdi Liu, Xiaoxue Cheng, Zhangyang Gao, Hong Chang, Cheng Tan, Shiguang Shan, and Xilin Chen. Protinvtree: Deliberate protein inverse folding with reward-guided tree search. *arXiv preprint arXiv:2506.00925*, 2025b.

Mingjie Liu, Shizhe Diao, Ximing Lu, Jian Hu, Xin Dong, Yejin Choi, Jan Kautz, and Yi Dong. Prorl: Prolonged reinforcement learning expands reasoning boundaries in large language models. *arXiv preprint arXiv:2505.24864*, 2025c.

Tianyu Liu, Yifei Zhang, Yanling Zhao, Shijie Geng, Chunyang Li, Jiangning Zhao, and Chengquan Yuan. Rlhf-v: Towards trustworthy mllms via behavior alignment from fine-grained correctional human feedback, 2024.

Isaac D Lutz, Shunzhi Wang, Christoffer Norn, Alexis Courbet, Andrew J Borst, Yan Ting Zhao, Annie Dosey, Longxing Cao, Jinwei Xu, Elizabeth M Leaf, et al. Top-down design of protein architectures with reinforcement learning. *Science*, 380(6642):266–273, 2023.

Tianyu Mi, Yuxiang Wang, Jingyu Zhao, Wanze Wang, Yunhao Shen, Nan Xiao, Ligong Chen, Guo-Qiang Chen, Shuyi Zhang, Wen-Bin Zhang, et al. Accelerating virtual directed evolution of proteins via reinforcement learning. *bioRxiv*, pp. 2025–06, 2025.

Noardeen Munsamy, Alexey Strokach, Philip Tran, and Philip M Kim. Zymctrl: a conditional language model for the controllable generation of artificial enzymes. *Nature Machine Intelligence*, 6:1–12, 2024. doi: 10.1038/s42256-024-00792-1.

Erik Nijkamp, Jeffrey A Ruffolo, Eli N Weinstein, Nikhil Naik, and Ali Madani. Progen2: exploring the boundaries of protein language models. *Cell Systems*, 14(11):968–978, 2023. doi: 10.1016/j.cels.2023.10.002.

Pascal Notin, Aaron Kollasch, Daniel Ritter, Lood Van Niekerk, Steffanie Paul, Han Spinner, Nathan Rollins, Ada Shaw, Rose Orenbuch, Ruben Weitzman, et al. Proteingym: Large-scale benchmarks for protein fitness prediction and design. *Advances in Neural Information Processing Systems*, 36: 64331–64379, 2023.

Tobias H Olsen, Fergus Boyles, and Charlotte M Deane. Ablang: an antibody language model for completing antibody sequences. *Bioinformatics Advances*, 2(1):vbac046, 2022. doi: 10.1093/bioadv/vbac046.

Jeffrey Ouyang-Zhang, Daniel Diaz, Adam Klivans, and Philipp Krähenbühl. Predicting a protein’s stability under a million mutations. *Advances in Neural Information Processing Systems*, 36: 76229–76247, 2023.

Ryan Park, Darren J Hsu, C Brian Roland, Maria Korshunova, Chen Tessler, Shie Mannor, Olivia Viessmann, and Bruno Trentini. Improving inverse folding for peptide design with diversity-regularized direct preference optimization. *arXiv preprint arXiv:2410.19471*, 2024.

Romain Paulus, Caiming Xiong, and Richard Socher. A deep reinforced model for abstractive summarization. *arXiv preprint arXiv:1705.04304*, 2017.

Malak Pirtskhalava, Anthony A Armstrong, Maia Grigolava, Mindia Chubinidze, Evgenia Alimbarashvili, Boris Vishnepolsky, Andrei Gabrielian, Alex Rosenthal, Darrell E Hurt, and Michael Tartakovsky. Dbaasp v3: database of antimicrobial/cytotoxic activity and structure of peptides as a resource for development of new therapeutics. *Nucleic acids research*, 49(D1):D288–D297, 2021.

Anna I Podgornaia and Michael T Laub. Pervasive degeneracy and epistasis in a protein-protein interface. *Science*, 347(6222):673–677, 2015.

Jiezhong Qiu, Junde Xu, Jie Hu, Hanqun Cao, Liya Hou, Zijun Gao, Xinyi Zhou, Anni Li, Xiujuan Li, Bin Cui, et al. Instructplm: Aligning protein language models to follow protein structure instructions. *bioRxiv*, pp. 2024–04, 2024.

Marc’Aurelio Ranzato, Sumit Chopra, Michael Auli, and Wojciech Zaremba. Sequence level training with recurrent neural networks. *arXiv preprint arXiv:1511.06732*, 2015.

Dingyi Rong, Haotian Lu, Wenzhuo Zheng, Fan Zhang, Shuangjia Zheng, and Ning Liu. Enerbridge-dpo: Energy-guided protein inverse folding with markov bridges and direct preference optimization. *arXiv preprint arXiv:2506.09496*, 2025.

Jeffrey A Ruffolo, Stephen Nayfach, Joseph Gallagher, Aadyot Bhatnagar, Joel Beazer, Riffat Husain, Jordan Russ, Jennifer Yip, Emily Hill, Martin Pacesa, et al. Design of highly functional genome editors by modelling crispr-cas sequences. *Nature*, pp. 1–8, 2025.

John Schulman, Filip Wolski, Prafulla Dhariwal, Alec Radford, and Oleg Klimov. Proximal policy optimization algorithms. *arXiv preprint arXiv:1707.06347*, 2017.

Joost Schymkowitz, Jesper Borg, Francois Stricher, Robby Nys, Frederic Rousseau, and Luis Serrano. The foldx web server: an online force field. *Nucleic acids research*, 33(suppl_2):W382–W388, 2005.

Darsh J. Shah et al. Rethinking reflection in pre-training. *arXiv preprint arXiv:2504.04022*, 2025.

Zhihong Shao, Peiyi Wang, Qihao Zhu, Runxin Xu, Junxiao Song, Xiao Bi, Haowei Zhang, Mingchuan Zhang, YK Li, Yang Wu, et al. Deepseekmath: Pushing the limits of mathematical reasoning in open language models. *arXiv preprint arXiv:2402.03300*, 2024.

Guobang Shi, Xinyue Kang, Fanyi Dong, Yanchao Liu, Ning Zhu, Yuxuan Hu, Hanmei Xu, Xingzhen Lao, and Heng Zheng. Dramp 3.0: an enhanced comprehensive data repository of antimicrobial peptides. *Nucleic acids research*, 50(D1):D488–D496, 2022.

Richard W Shuai, Jeffrey A Ruffolo, and Jeffrey J Gray. IgIm: Infilling language modeling for antibody sequence design. *Cell Systems*, 14(11):979–989, 2023. doi: 10.1016/j.cels.2023.10.001.

Ian Sillitoe, Nicola Bordin, Natalie Dawson, Vaishali P Waman, Paul Ashford, Harry M Scholes, Camilla SM Pang, Laurel Woodridge, Clemens Rauer, Neeladri Sen, et al. Cath: increased structural coverage of functional space. *Nucleic acids research*, 49(D1):D266–D273, 2021.

Sarah Sirin, James R Apgar, Eric M Bennett, and Amy E Keating. Ab-bind: antibody binding mutational database for computational affinity predictions. *Protein Science*, 25(2):393–409, 2016.

Martin Steinegger and Johannes Söding. Mmseqs2 enables sensitive protein sequence searching for the analysis of massive data sets. *Nature biotechnology*, 35(11):1026–1028, 2017.

Jin Su, Chenchen Han, Yuyang Zhou, Junjie Shan, Xibin Zhou, and Fajie Yuan. Saprot: Protein language modeling with structure-aware vocabulary, 2023.

Haoran Sun, Liang He, Pan Deng, Guoqing Liu, Zhiyu Zhao, Yuliang Jiang, Chuan Cao, Fusong Ju, Lijun Wu, Haiguang Liu, et al. Accelerating protein engineering with fitness landscape modelling and reinforcement learning. *Nature Machine Intelligence*, pp. 1–15, 2025.

Xiangru Tang, Howard Dai, Elizabeth Knight, Fang Wu, Yunyang Li, Tianxiao Li, and Mark Gerstein. A survey of generative ai for de novo drug design: new frontiers in molecule and protein generation. *Briefings in Bioinformatics*, 25(4), 2024.

Timothy Truong Jr and Tristan Bepler. Poet: A generative model of protein families as sequences-of-sequences. *Advances in Neural Information Processing Systems*, 36:77379–77415, 2023.

Yannick Vogt, Mehdi Naouar, Maria Kalweit, Christoph Cornelius Miethling, Justus Duyster, Joschka Boedecker, and Gabriel Kalweit. Betterbodies: Reinforcement learning guided diffusion for antibody sequence design. *CoRR*, 2024.

Chenyu Wang, Masatoshi Uehara, Yichun He, Amy Wang, Avantika Lal, Tommi Jaakkola, Sergey Levine, Aviv Regev, Tommaso Biancalani, et al. Fine-tuning discrete diffusion models via reward optimization with applications to dna and protein design. In *The Thirteenth International Conference on Learning Representations*.

Fanhao Wang, Tiantian Zhang, Jintao Zhu, Xiaoling Zhang, Changsheng Zhang, and Luhua Lai. Reinforcement learning-based target-specific de novo design of cyclic peptide binders. *Journal of Medicinal Chemistry*, 2025a.

Guangshun Wang, Xia Li, and Zhe Wang. Apd3: the antimicrobial peptide database as a tool for research and education. *Nucleic acids research*, 44(D1):D1087–D1093, 2016.

Menglun Wang, Zixuan Cang, and Guo-Wei Wei. A topology-based network tree for the prediction of protein–protein binding affinity changes following mutation. *Nature Machine Intelligence*, 2(2):116–123, 2020.

Yi Wang, Hui Tang, Lichao Huang, Lulu Pan, Lixiang Yang, Huanming Yang, Feng Mu, and Meng Yang. Self-play reinforcement learning guides protein engineering. *Nature Machine Intelligence*, 5(8):845–860, 2023.

Yuhao Wang, Qiang Zhang, Ming Qin, Xiang Zhuang, Xiaotong Li, Zhichen Gong, Zeyuan Wang, Yu Zhao, Jianhua Yao, Keyan Ding, et al. Knowledge-aware reinforced language models for protein directed evolution. In *Forty-first International Conference on Machine Learning*, 2024.

Ziwen Wang, Jiajun Fan, Ruihan Guo, Thao Nguyen, Heng Ji, and Ge Liu. Proteinzero: Self-improving protein generation via online reinforcement learning. *arXiv preprint arXiv:2506.07459*, 2025b.

Xumeng Wen, Zihan Liu, Shun Zheng, Zhijian Xu, Shengyu Ye, Zhirong Wu, Xiao Liang, Yang Wang, Junjie Li, Ziming Miao, Jiang Bian, and Mao Yang. Reinforcement learning with verifiable rewards implicitly incentivizes correct reasoning in base llms, 2025. URL <https://arxiv.org/abs/2506.14245>.

Fang Wu and Yejin Choi. On the limits of rlvr: Support, entropy, and the illusion of reasoning. In *2nd AI for Math Workshop@ ICML 2025*.

Fang Wu and Stan Z Li. A hierarchical training paradigm for antibody structure-sequence co-design. *Advances in Neural Information Processing Systems*, 36:31140–31157, 2023.

Fang Wu, Lirong Wu, Dragomir Radev, Jinbo Xu, and Stan Z Li. Integration of pre-trained protein language models into geometric deep learning networks. *Communications Biology*, 6(1):876, 2023.

Fang Wu, Weihao Xuan, Ximing Lu, Zaid Harchaoui, and Yejin Choi. The invisible leash: Why rlvr may not escape its origin. *arXiv preprint arXiv:2507.14843*, 2025.

Ziwei Wu, Yang Zhang, and Hongyan Li. Maye: A transparent rl framework for vision-language models, 2024.

Yijia Xiao, Edward Sun, Tong Chen, Fang Wu, Di Luo, and Wei Wang. Trading-r1: Financial trading with llm reasoning via reinforcement learning. *arXiv preprint arXiv:2509.11420*, 2025.

Junde Xu, Zijun Gao, Xinyi Zhou, Jie Hu, Xingyi Cheng, Le Song, Guangyong Chen, Pheng-Ann Heng, and Jiezhong Qiu. Protein inverse folding from structure feedback. *arXiv preprint arXiv:2506.03028*, 2025.

Minghao Xu, Xinyu Yuan, Santiago Miret, and Jian Tang. Protst: Multi-modality learning of protein sequences and biomedical texts. In *International Conference on Machine Learning*, pp. 38749–38767. PMLR, 2023a.

Xiaopeng Xu, Tiantian Xu, Juxiao Zhou, Xingyu Liao, Ruochi Zhang, Yu Wang, Lu Zhang, and Xin Gao. Ab-gen: antibody library design with generative pre-trained transformer and deep reinforcement learning. *Genomics, Proteomics & Bioinformatics*, 21(5):1043–1053, 2023b.

Fanglei Xue, Andrew Kubaney, Zhichun Guo, Joseph K Min, Ge Liu, Yi Yang, and David Baker. Improving protein sequence design through designability preference optimization. *arXiv preprint arXiv:2506.00297*, 2025.

Jason Yang, Ravi G Lal, James C Bowden, Raul Astudillo, Mikhail A Hameedi, Sukhvinder Kaur, Matthew Hill, Yisong Yue, and Frances H Arnold. Active learning-assisted directed evolution. *Nature Communications*, 16(1):714, 2025.

Kevin K Yang, Zachary Wu, and Frances H Arnold. Machine-learning-guided directed evolution for protein engineering. *Nature methods*, 16(8):687–694, 2019.

Yang Yue, Zhiqi Chen, Rui Lu, Andrew Zhao, Zhaokai Wang, Shiji Song, and Gao Huang. Does reinforcement learning really incentivize reasoning capacity in llms beyond the base model? *arXiv preprint arXiv:2504.13837*, 2025.

Hao Zhang, Wei Li, Zhi Jin, Xiaoying Luo, Nan Yang, and Zenglin Chen. Enhancing code llms with reinforcement learning in code generation: A survey, 2024a.

Haoxuan Zhang, Dianbo Yu, and Shimon Whiteson. Grpo-lead: A difficulty-aware reinforcement learning approach for concise mathematical reasoning in language models, 2024b.

Lei Zhang, Jianhua Wang, and Xiaofeng Li. Deep reinforcement learning-based dialogue policy with graph convolutional q-network. *Proceedings of the Language Resources and Evaluation Conference*, pp. 4681–4688, 2024c.

Qiang Zhang, Wanyi Chen, Ming Qin, Yuhao Wang, Zhongji Pu, Keyan Ding, Yuyue Liu, Qunfeng Zhang, Dongfang Li, Xinjia Li, et al. Integrating protein language models and automatic biofoundry for enhanced protein evolution. *Nature Communications*, 16(1):1553, 2025.

Yang Zhang and Jeffrey Skolnick. Tm-align: a protein structure alignment algorithm based on the tm-score. *Nucleic acids research*, 33(7):2302–2309, 2005.

Yang Zhang, Wei Li, Kai Chen, and Honggang Liu. Memprotmd: Membrane protein molecular dynamics with machine learning, 2024d.

Rosie Zhao et al. Echo chamber: RL post-training amplifies behaviors learned in pretraining. *arXiv preprint arXiv:2504.07912*, 2025.

A IMPLEMENTATION DETAILS

A.1 PROTEIN INVERSE FOLDING

Training Details Following (Xu et al., 2025), the DPO framework used $\beta = 0.5$ to balance reference model retention with preference adaptation, and regularization weight $\lambda = 1$ for optimal learning from chosen and rejected sequence pairs. Training employed AdamW optimizer with learning rate 1×10^{-5} , $\beta_1 = 0.9$, $\beta_2 = 0.999$, $\epsilon = 1 \times 10^{-8}$, and batch size 128 across 8 NVIDIA A100 GPUs. LoRA adaptation used rank $r = 16$ and $\alpha = 16$, training only 0.1% of total parameters.

Single-round training used 4,000 steps with 20 sequences per structure, while multi-round training employed 200 steps per round across 20 rounds using 200 sequences per structure. The reference model π_{ref} was reinitialized with previous iteration weights during multi-round training to maintain preference alignment and prevent catastrophic forgetting.

Sampling Details Sequence generation employed distinct sampling parameters for training and evaluation phases. For **Training**, single-round training used `temperature=1.0` and `top-p=0.9` to generate 20 sequences per structure, while multi-round training utilized more exploratory parameters (`temperature=1.1`, `top-p=1.0`) with 200 sequences per structure to encourage broader search space exploration. For **evaluation**, temperature was reduced to `temperature=0.15` with 128 sequences per structure to ensure reproducible comparisons across benchmarks.

A.2 ANTIMICROBIAL PEPTIDE DESIGN

Training Details Following (Cao et al., 2025b), the PPO framework applied learning rate 1×10^{-5} , increased batch size to 256, and reduced training to 10 epochs over 3000 steps. The ApexMIC predictor employed ESM2 embeddings processed through multi-layer perceptron architecture, trained using Focal Loss with focusing parameter γ and class weighting α_i to address dataset imbalance. The base ProGen2-xlarge model (6.4B parameters) underwent supervised fine-tuning using LoRA adaptation with rank 32, alpha 16, dropout 0.1, learning rate 1×10^{-4} , and batch size 16 over 30 epochs.

Sampling Details Sequence generation employed `temperature=1.0`, `top-p=0.95`, `beam number=4`, `length penalty=1.2`, and `repetition penalty=1.2` with `maximum length=50`. It also excluded invalid amino acids (B, O, U, X, Z) and maintained consistent sequence length constraints. The sampling strategy ensured diverse peptide generation while preserving antimicrobial sequence patterns learned during fine-tuning. During evaluation, 131,072 (4096*32) and 160,000 AMP sequences are generated for `pass@k`-related metric and latent visualization, respectively.

A.3 KINASE MUTATION

Training details Following (Wang et al., 2024), we applied learning rate 1×10^{-5} , batch 16. We set the maximum total steps to 10,000 and created 50 parallel environments for training. The entropy-loss coefficient is set to 0. To prevent the policy from being trapped in local optima, we set the discount factor to 0 so that only the reward of the final sequence is used. The PPO clipping ratio is 0.2 and the sampling temperature is 1.0. Reward is the experimentally measured fitness from the dataset; sequences not present in the dataset receive -1, and invalid sequences receive -100.

Sampling details During sampling, we used `temperature=1.0` and `top-p=1.0`, and created a single environment to perform 50,000 rounds of sampling. Following the same protocol as in training, mutation was terminated—and the result saved—either when the maximum number of mutation steps was reached or when the sequence’s fitness exceeded the initial fitness. After each sample was completed, the environment was re-initialized by randomly selecting a new starting sequence from the test set for the next round of mutation.

A.4 ANTIBODY MUTATION

Training details During training, we used a fixed random seed as 42 and optimize with Adam ($lr=4 \times 10^{-5}$, weight decay= 1×10^{-4}), batch size 32, and global gradient clipping at 0.5 for 30 epochs. Training is conducted on 4 A100 GPUs. In RL fine-tuning, we performed on-policy multi-step rollouts ($T = 4$) and restrict edits to CDR-masked positions. At each step, up to four sites are mutated while disallowing the wild-type residue; sites are selected greedily from position probabilities, and amino acids are chosen as the non-wild-type arg max under temperature-scaled logits. Both amino-acid and position temperatures linearly anneal from 1.0 to 0.5 over the first 1,000 steps. Advantages/returns are computed with GAE ($\gamma = 0.99$, $\lambda = 0.95$), returns are standardized, and GRPO rank normalization is applied to advantages. We optimize a PPO objective with clipping 0.2; the log-probability sums amino-acid and position terms with weight 0.5 on the position term:

$$\log \pi = \log \pi_{AA} + 0.5 \log \pi_{pos}.$$

The loss weight for KL loss (α), value loss (β), and entropy loss (γ) are 20.0, 0.4, and 0.01, respectively. KL was computed only at mutated sites; and the final KL term is clipped to ≤ 10.0 . Sequences and masks use `pad_id=1`.

Sampling details We generate each antibody sequence we mutate up to K sites (default $K = 4$); site choice and residue replacement are driven by the model’s position propensities and amino-acid logits with `temperature=1.0`, `position_temp=1.0`, and `position_threshold=0.5`. A frozen reward model predicted ddG for each mutant and can optionally score the wild type. Inference was conducted on a single A100 GPU, default `batch_size=16`.

B DATASET AND EVALUATION METRICS

B.1 KINASE MUTATION

Datasets We evaluate the impact of RL training on protein mutations using the PhoQ dataset(Podgornaia & Laub (2015)). This dataset provides 140,517 annotated data points among the 160,000 possible variants that differ at four mutational sites (A284,V285, S288, T289). Fitness is reported as the corresponding phosphatase or kinase activity for each PhoQ variant. For the remaining unlabeled variants, we follow the convention in Wang et al. (2024) and assign a fitness value of -1. Following the fitness-split protocol of (Ouyang-Zhang et al. (2023)), we fixed the fourth site and partitioned the first three positions into training and test sets in an 8:2 ratio. All sequences were then assigned to four bins according to their fitness values ($=0, \leq 1, \leq 10, > 10$). From each bin we randomly sampled 100 sequences in both the training and test splits to form the initial-seed pools.

Evaluation metrics **Positional entropy** is calculated as the Shannon entropy at each of the first three mutable positions of the mutated sequence.

B.2 ANTIBODY MUTATION

Datasets we utilized AB1101 (Sirin et al., 2016), an open-source dataset comprising 32 antigen-antibody complexes with comprehensive mutational sequence data. This dataset contains 645 single-point mutation entries and 456 multi-point mutation entries. Following the data partitioning strategy established in ProtAttBA, we employed single-point mutations as training data for both the policy model and reward model, while reserving multi-point mutations for testing purposes. For reinforcement learning training, we performed additional stratification of the multi-point mutation data based on complex PDB identifiers. Through random selection, we designated 1MLC and 1VFB as the test PDB structures to ensure robust evaluation of our approach.

Evaluation metrics **Positional Entropy** is calculated based on the Shannon entropy at each individual position within the CDR of the mutated antibody sequences. **Perplexity** is computed as the exponential of the average negative log-likelihood of the generated protein sequences under a specific model.

B.3 AMP DESIGN

Datasets Following the ApexAmphion framework (Cao et al., 2025b), we trained a reward model utilizing currently available open-source MIC values sourced from three established databases: DBAASP (Pirtskhalava et al., 2021), DRAMP (Shi et al., 2022), and APD3 (Wang et al., 2016). We selected sequences with lengths ranging from 8 to 50 amino acids and classified them as active peptides based on MIC values below $32 \mu\text{M/mL}$. This process yielded a total of 7,888 samples encompassing both positive and negative instances. To ensure proper data partitioning and minimize sequence similarity bias, we employed MMseqs2 (Steinegger & Söding, 2017) for clustering and dataset splitting, resulting in a training, validation, and test distribution of 6153, 789, and 946 samples, respectively.

Evaluation metrics **Diversity** is calculated as the average sequence similarity between generated sequences, measuring the model’s ability to produce varied outputs and avoid mode collapse. **Novelty** is computed based on the degree of novelty between generated sequences and natural sequences, specifically defined as the average of (1 - maximum sequence similarity) across all generated sequences, where the maximum similarity represents the highest identity score between each generated sequence and any reference natural sequence. **Perplexity** is computed as the exponential of the average negative log-likelihood of the generated protein sequences under a specific model.

B.4 PROTEIN INVERSE FOLDING

Datasets The dataset construction leverages CATH4.2 (Sillitoe et al., 2021), following to the official train-test split scheme established by the CATH database. Both the base model training and DPO dataset construction are exclusively conducted on the training partition, which comprises 18,024 protein structures. Model performance evaluation is carried out on the CATH4.2 test set containing 1,120 structures, supplemented by two additional evaluation benchmarks: TS50 and TS500, which contain 50 and 470 protein structures respectively. This evaluation framework ensures comprehensive assessment across diverse structural complexity and provides robust validation of the model’s generalization capabilities.

Evaluation metrics **Diversity** is calculated as the average sequence similarity between generated sequences, measuring the model’s ability to produce varied outputs and avoid mode collapse. **Novelty** is computed based on the degree of novelty between generated sequences and natural sequences, specifically defined as the average of (1 - maximum sequence similarity) across all generated sequences, where the maximum similarity represents the highest identity score between each generated sequence and any reference natural sequence. **Perplexity** is computed as the exponential of the average negative log-likelihood of the generated protein sequences under a specific model. **Recovery Rate** is computed as the percentage of amino acid positions that are correctly predicted compared to the native sequence. **TM-Score** evaluates the structural similarity between predicted and native structures by measuring the geometric alignment quality across all residue positions.

C METHOD DETAILS

C.1 ANTIBODY MUTATION NETWORK

Algorithm 1 ProtAttBA-improved: Antibody-antigen Binding Affinity Prediction and Featurization

Require: Wild-type antibody sequence S_{ab}^{wt} , mutant antibody sequence S_{ab}^{mt}
Require: Wild-type antigen sequence S_{ag}^{wt} , mutant antigen sequence S_{ag}^{mt}
Require: Attention masks $M_{ab}^{wt}, M_{ab}^{mt}, M_{ag}^{wt}, M_{ag}^{mt}$
Ensure: Binding affinity prediction \hat{y} and auxiliary outputs

- 1: // **Step 1: Protein Language Model Encoding**
- 2: $E_{ab}^{wt} \leftarrow \text{ESM}(S_{ab}^{wt}, M_{ab}^{wt}) \in \mathbb{R}^{B \times L_{ab} \times H}$ {Wild-type antibody embeddings}
- 3: $E_{ab}^{mt} \leftarrow \text{ESM}(S_{ab}^{mt}, M_{ab}^{mt}) \in \mathbb{R}^{B \times L_{ab} \times H}$ {Mutant antibody embeddings}
- 4: $E_{ag}^{wt} \leftarrow \text{ESM}(S_{ag}^{wt}, M_{ag}^{wt}) \in \mathbb{R}^{B \times L_{ag} \times H}$ {Wild-type antigen embeddings}
- 5: $E_{ag}^{mt} \leftarrow \text{ESM}(S_{ag}^{mt}, M_{ag}^{mt}) \in \mathbb{R}^{B \times L_{ag} \times H}$ {Mutant antigen embeddings}
- 6: // **Step 2: Attention-based Feature Enhancement**
- 7: **for** $x \in \{E_{ab}^{wt}, E_{ab}^{mt}, E_{ag}^{wt}, E_{ag}^{mt}\}$ **do**
- 8: $x' \leftarrow \text{AttnTransform}(x) = \text{softmax}(\text{Conv1D}(\text{LayerNorm}(x))) \odot x$ {Enhanced features}
- 9: **end for**
- 10: // **Step 3: Cross-Modal Attention Mechanism**
- 11: $\tilde{E}_{ag}^{wt} \leftarrow \text{MultiHeadAttn}(E_{ag}^{wt}, E_{ab}^{wt}, E_{ab}^{wt}, M_{ab}^{wt})$ {Antigen attends to antibody}
- 12: $\tilde{E}_{ag}^{mt} \leftarrow \text{MultiHeadAttn}(E_{ag}^{mt}, E_{ab}^{mt}, E_{ab}^{mt}, M_{ab}^{mt})$ {Mutant antigen-antibody attention}
- 13: $\tilde{E}_{ab}^{wt} \leftarrow \text{MultiHeadAttn}(E_{ab}^{wt}, E_{ag}^{wt}, E_{ag}^{wt}, M_{ag}^{wt})$ {Antibody attends to antigen}
- 14: $\tilde{E}_{ab}^{mt} \leftarrow \text{MultiHeadAttn}(E_{ab}^{mt}, E_{ag}^{mt}, E_{ag}^{mt}, M_{ag}^{mt})$ {Mutant antibody-antigen attention}
- 15: // **Step 4: Auxiliary Classification Heads**
- 16: $L_{ab}^{wt} \leftarrow \text{Linear}(\tilde{E}_{ab}^{wt}) \in \mathbb{R}^{B \times L_{ab} \times 33}$ {Wild-type antibody logits}
- 17: $L_{ab}^{mt} \leftarrow \text{Linear}(\tilde{E}_{ab}^{mt}) \in \mathbb{R}^{B \times L_{ab} \times 33}$ {Mutant antibody logits}
- 18: $L_{ag}^{wt} \leftarrow \text{Linear}(\tilde{E}_{ag}^{wt}) \in \mathbb{R}^{B \times L_{ag} \times 33}$ {Wild-type antigen logits}
- 19: $L_{ag}^{mt} \leftarrow \text{Linear}(\tilde{E}_{ag}^{mt}) \in \mathbb{R}^{B \times L_{ag} \times 33}$ {Mutant antigen logits}
- 20: // **Step 5: Attention-weighted Global Pooling**
- 21: $h_{ab}^{wt} \leftarrow \text{AttnMean}(\tilde{E}_{ab}^{wt}, M_{ab}^{wt}) \in \mathbb{R}^{B \times H}$ {Pooled antibody representation}
- 22: $h_{ab}^{mt} \leftarrow \text{AttnMean}(\tilde{E}_{ab}^{mt}, M_{ab}^{mt}) \in \mathbb{R}^{B \times H}$ {Pooled mutant antibody}
- 23: $h_{ag}^{wt} \leftarrow \text{AttnMean}(\tilde{E}_{ag}^{wt}, M_{ag}^{wt}) \in \mathbb{R}^{B \times H}$ {Pooled antigen representation}
- 24: $h_{ag}^{mt} \leftarrow \text{AttnMean}(\tilde{E}_{ag}^{mt}, M_{ag}^{mt}) \in \mathbb{R}^{B \times H}$ {Pooled mutant antigen}
- 25: // **Step 6: Complex Formation and Prediction**
- 26: $h^{wt} \leftarrow h_{ab}^{wt} + h_{ag}^{wt}$ {Wild-type complex representation}
- 27: $h^{mt} \leftarrow h_{ab}^{mt} + h_{ag}^{mt}$ {Mutant complex representation}
- 28: $h_{concat} \leftarrow \text{Concat}(h^{wt}, h^{mt}) \in \mathbb{R}^{B \times 2H}$ {Concatenated complexes}
- 29: $h_{norm} \leftarrow \text{BatchNorm}(h_{concat})$ {Normalized features}
- 30: // **Step 7: Multi-layer Prediction Head**
- 31: $h_1 \leftarrow \text{Tanh}(\text{Linear}(h_{norm})) \in \mathbb{R}^{B \times H/2}$ {First hidden layer}
- 32: $h_1 \leftarrow \text{Dropout}(h_1, p = 0.1)$ {Apply dropout}
- 33: $h_2 \leftarrow \text{ReLU}(\text{Linear}(h_1)) \in \mathbb{R}^{B \times H/2}$ {Second hidden layer}
- 34: $\hat{y} \leftarrow \text{Linear}(h_2) \in \mathbb{R}^B$ {Binding affinity prediction}
- 35: **return** $\hat{y}, L_{ab}^{wt}, L_{ag}^{wt}, L_{ab}^{mt}, L_{ag}^{mt}$

C.2 ANTIBODY MUTATION STRATEGY

Algorithm 2 Policy-Guided Antibody Mutation

Require: Policy model position probabilities $P_{pos} \in \mathbb{R}^L$
Require: Mutation model logits $L_{mut} \in \mathbb{R}^{L \times V}$
Require: Wild-type sequence S_{wt} , CDR mask M_{cdr}
Require: Temperature τ , stochastic flag s

- 1: $P_{masked} \leftarrow P_{pos} \odot M_{cdr}$ {Mask to CDR}
- 2: **Position Selection:**
- 3: **if** $s = \text{True}$ **then**
- 4: Select positions where $P_{masked} > \theta$ via multinomial sampling {**Stochastic inference**}
- 5: **else**
- 6: Select top- k positions by P_{masked} values {**Deterministic training**}
- 7: **end if**
- 8: **Amino Acid Mutation:**
- 9: **for** each selected position i **do**
- 10: $P_{aa} \leftarrow \text{softmax}(L_{mut}[i]/\tau)$ {Apply temperature}
- 11: $P_{aa}[S_{wt}[i]] \leftarrow 0$ {Mask wild-type residue}
- 12: $P_{aa} \leftarrow P_{aa} / \sum P_{aa}$ {Re-normalize}
- 13: **if** $s = \text{True}$ **then**
- 14: $S_{mut}[i] \leftarrow \text{sample}(P_{aa})$ {Stochastic sampling}
- 15: **else**
- 16: $S_{mut}[i] \leftarrow \arg \max(P_{aa})$ {Greedy selection}
- 17: **end if**
- 18: **end for**
- 19: **return** Mutated sequence S_{mut}

C.3 KINASE MUTATION STRATEGY

Algorithm 3 Kinase Mutation

Require: Initial sequence $S_0 \in \mathbb{Z}^L$, Pretrained ESM Encoder f_{ESM} , Action Network f_{Action} , Value Network f_{Value} , Masked Language Model f_{MLM} , Tokenizer T , Mutation positions $P = \{p_1, p_2, p_3\}$, Amino acid vocabulary \mathbb{A} .

Ensure: Final mutated sequence S_N .

- 1: **// Initialization**
- 2: $S_{obs} \leftarrow S_0$ {Initialize observation with the starting sequence}
- 3: $E_{ref} \leftarrow f_{ESM}(S_{protein})$ {Get reference embedding for normalization}
- 4: **for** $t = 0$ to $N - 1$ **do**
- 5: **// Step 1: Sequence Feature Extraction**
- 6: $E_t \leftarrow f_{ESM}(S_{obs}) \in \mathbb{R}^{B \times L \times H}$ {Encode current sequence}
- 7: $E'_t \leftarrow E_t / (E_{ref} + \epsilon)$ {Normalize embeddings}
- 8: $E_{flat} \leftarrow \text{Flatten}(E'_t) \in \mathbb{R}^{B \times (L \cdot H)}$ {Flatten for policy networks}
- 9: **// Step 2: Select Mutation Position (Actor)**
- 10: $l_{pos} \leftarrow f_{Action}(E_{flat}) \in \mathbb{R}^{B \times |P|}$ {Get logits for positions}
- 11: $\pi_{pos} \leftarrow \text{Categorical}(\text{logits} = l_{pos})$ {Create position distribution}
- 12: $idx_p \leftarrow \pi_{pos}.\text{sample}()$ {Sample position index, e.g., 0, 1, or 2}
- 13: $p_t \leftarrow P[idx_p]$ {Map index to actual sequence position, e.g., 96, 97, 100}
- 14: **// Step 3: Predict Candidate Amino Acid (Masked LM)**
- 15: $S_{mask} \leftarrow S_{obs}; S_{mask}[p_t] \leftarrow \text{MASK_TOKEN}$ {Mask selected position}
- 16: $l_{aa} \leftarrow f_{MLM}(S_{mask})[p_t] \in \mathbb{R}^{|\mathbb{A}|}$ {Get logits for amino acids at position p_t }
- 17: $\pi_{aa} \leftarrow \text{Softmax}(l_{aa}/\tau)$ {Create amino acid distribution with temperature τ }
- 18: $a_t \leftarrow \pi_{aa}.\text{sample}()$ {Sample a new amino acid token}
- 19: **// Step 4: Update Sequence and Get Reward**
- 20: $S_{new} \leftarrow S_{obs}; S_{new}[p_t] \leftarrow a_t$ {Apply mutation}
- 21: $R_t, \text{done} \leftarrow \text{PhoQEnv.step}(S_{new})$ {Get reward from environment}
- 22: $S_{obs} \leftarrow S_{new}$ {Update the state for the next iteration}
- 23: **end for**
- 24: **return** S_{obs}

C.4 REINFORCEMENT LEARNING LOSS FOR AMP DESIGN

We employ three widely used RL algorithms to fine-tune PLMs $p_\theta(\mathbf{s})$ parameterized by θ , each targeting different aspects of biological knowledge acquisition.

Direct Preference Optimization (DPO) DPO learns from preference pairs without explicit reward modeling. Given preference dataset $\mathcal{D} = \{(\mathbf{s}_i^+, \mathbf{s}_i^-)\}$ where $\mathbf{s}_i^+ \succ \mathbf{s}_i^-$, the DPO loss is:

$$\mathcal{L}_{DPO}(\theta) = -\mathbb{E}_{(\mathbf{s}^+, \mathbf{s}^-) \sim \mathcal{D}} \left[\log \sigma \left(\beta \log \frac{p_\theta(\mathbf{s}^+)}{p_{ref}(\mathbf{s}^+)} - \beta \log \frac{p_\theta(\mathbf{s}^-)}{p_{ref}(\mathbf{s}^-)} \right) \right],$$

where p_{ref} is the reference model, $\beta > 0$ controls KL divergence, and σ is the sigmoid function.

Proximal Policy Optimization (PPO) PPO optimizes the policy using clipped importance sampling. For sequence \mathbf{s} with reward

$$\mathcal{L}_{PPO}(\theta) = \mathbb{E}_{\mathbf{s} \sim p_{\theta_{old}}} \left[\min \left(\rho_\theta(\mathbf{s}) \hat{A}(\mathbf{s}), \text{clip}(\rho_\theta(\mathbf{s}), 1 - \epsilon, 1 + \epsilon) \hat{A}(\mathbf{s}) \right) \right] + \beta \cdot \mathbb{E}_{\mathbf{s} \sim p_\theta} [D_{KL}(p_\theta(\mathbf{s}) || p_{\theta_{old}}(\mathbf{s}))],$$

where $\rho_\theta(\mathbf{s}) = \frac{p_\theta(\mathbf{s})}{p_{\theta_{old}}(\mathbf{s})}$ represents the **importance ratio**, which measures the change in probability of a sequence between the current and the old policy. The term $\hat{A}(\mathbf{s})$ is the **advantage estimate**, which quantifies how much better or worse the current action is compared to the baseline. The parameter ϵ is the **clipping parameter**, which ensures that the policy update does not change too drastically. To prevent large policy updates, the loss includes the **Kullback-Leibler (KL) divergence**, denoted as $D_{KL}(p_\theta(\mathbf{s}) || p_{\theta_{old}}(\mathbf{s}))$, which measures deviation from the old policy to the current policy. Finally, β denotes a **hyperparameter** that controls the strength of the KL regularization.

Group Relative Policy Optimization (GRPO) GRPO computes relative advantages within sequence groups, making it suitable for comparative protein design. For group $\mathcal{G} = \{\mathbf{s}_1, \dots, \mathbf{s}_m\}$, the relative advantage is:

$$\hat{A}^{rel}(\mathbf{s}_j) = R(\mathbf{s}_j) - \frac{1}{m} \sum_{i=1}^m R(\mathbf{s}_i)$$

The GRPO loss extends PPO with group-wise normalization:

$$\begin{aligned} \mathcal{L}_{GRPO}(\theta) = & \mathbb{E}_{\mathcal{G}} \left[\frac{1}{|\mathcal{G}|} \sum_{\mathbf{s} \in \mathcal{G}} \min \left(\rho_\theta(\mathbf{s}) \hat{A}^{rel}(\mathbf{s}), \text{clip}(\rho_\theta(\mathbf{s}), 1 - \epsilon, 1 + \epsilon) \hat{A}^{rel}(\mathbf{s}) \right) \right] \\ & + \gamma \cdot \mathbb{E}_{\mathbf{s} \sim \pi_\theta} [D_{KL}(p_\theta(\mathbf{s}) || p_{\theta_{old}}(\mathbf{s}))], \end{aligned}$$

where $\hat{A}^{rel}(\mathbf{s}_j)$ represents the **relative advantage** of sequence \mathbf{s}_j within the group \mathcal{G} . The importance ratio, denoted as $\rho_\theta(\mathbf{s}) = \frac{p_\theta(\mathbf{s})}{p_{\theta_{old}}(\mathbf{s})}$, measures the change in probability of a sequence between the current and old policies. The clipping parameter ϵ ensures that the policy update remains within a bounded range, preventing large, destabilizing changes. The **KL divergence** is regularized to avoid large policy updates. Finally, γ denotes the hyperparameter that controls the strength of the KL regularization.

D SUPPLEMENTARY EXPERIMENTAL RESULTS OF ANTIBODY MUTATION

D.1 TEST RESULTS ON THE RE-IMPLEMENTED PROTATTBA

Method	RMSE	Pearson cor.	Spearman cor.
ProtAttBA (Original)	2.10	0.55	0.45
ProtAttBA (Ours)	1.50	0.58	0.47

D.2 DISTRIBUTION SHIFT OF PREDICTED DDG

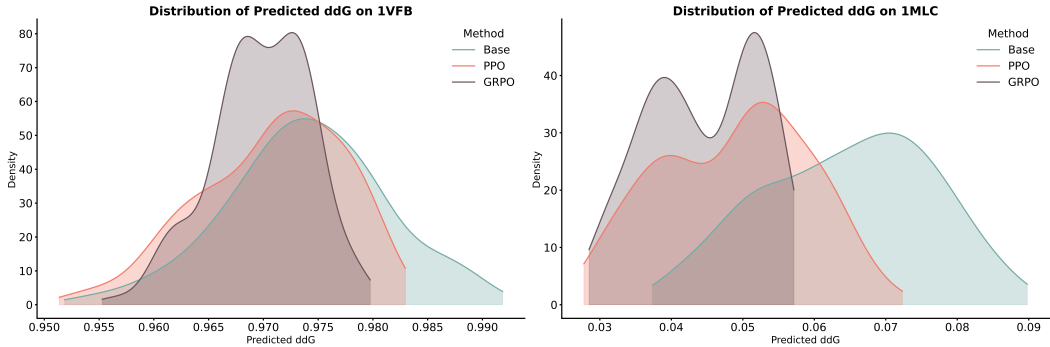


Figure 6: Predicted ddG distribution on test set PDBs.

E SUPPLEMENTARY EXPERIMENTAL RESULTS OF INVERSE FOLDING

E.1 ABLATION ON SUPPORT METRIC OF K

Table 2: Results for *Support* metric for four biological systems.

	Preservation	Expansion	Shrinkage	Out-Of-Support	ESR \uparrow
k=128	891	9	21	199	2.33
k=32	886	12	23	199	1.92
k=8	865	23	27	205	1.17
k=2	831	31	33	225	1.06

E.2 LATENT VISUALIZATION OF SUPPORT SUBSETS

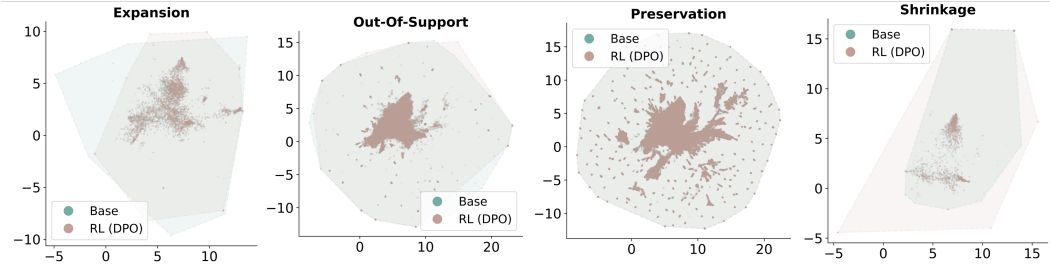


Figure 7: Latent visualization on inverse folding tasks for different support subsets.

F SUPPLEMENTARY EXPERIMENTAL RESULTS OF AMP DESIGN

F.1 BINARY CLASSIFICATION PERFORMANCE OF REWARD MODEL

Table 3: Results for ApexMIC on binary classification.

	Accuracy	Precision	Sensitivity	Specificity	F1-score	AUC-ROC
ApexMIC	0.96	0.62	0.82	0.98	0.70	0.90

G SUMMARY OF REINFORCEMENT LEARNING-GUIDED PROTEIN DESIGN METHODS

Table 4: Taxonomy of RL approaches in protein design.

Task	Method	RL Algorithm	Reward Function	Designed Biological Entity
Structural Design	Issac et al. (Lutz et al., 2023)	MCTS	Composite structural score: architecture/topology fit, sterics, geometry constraints	Symmetric multi-subunit protein assemblies
	GAPN (Gao et al., 2024)	PPO	Direct docking reward (pose/energy), adversarial reward to improve global assembly rules	Multimer protein complex assembly / docking paths
Sequence Optimization	EvoPlay (Wang et al., 2023)	MCTS (AlphaZero)	Task-specific predicted fitness/activity (surrogate property predictors)	Enzymes / general proteins
	RLXF (Blalock et al., 2025)	PPO	Experimentally measured function (e.g., fluorescence/fitness)	Diverse protein families (e.g., CreiLOV variants)
	μ Protein (Sun et al., 2025)	PPO	Predicted/experimental fitness from landscape model	Enzymes (e.g., β -lactamase)
Inverse Folding	RelaVDEP (Mi et al., 2025)	MCTS	Fine-tuned SPIRED-Fitness; structure/foldability filters (ESMFold/AF2 pLDDT, SPIRED-Stab $\Delta\Delta G/\Delta T_m$); diversity–fitness metric	GFP (fluorescence), NUDT15/VKOR1 (cellular abundance), AmeR (fold repression), PETase (enzymatic activity)
	ApexAmphion (Cao et al., 2025b)	PPO	Predicted MIC, physicochemical properties	Board-spectrum antimicrobial peptides
	ProteinZero (Wang et al., 2025b)	PPO, GRPO	ESM-Fold structural fidelity, $\Delta\Delta G$ stability proxy, diversity	General protein sequences

Continued on next page

Task	Method / Paper	RL Algorithm	Reward Function	Designed Entity
Protein Design	Xu et al. (Xu et al., 2025)	Multi-round DPO	TM-score	General protein sequences
	EnerBridge-DPO (Rong et al., 2025)	DPO	Energy score	Protein complex sequences
	ResiDPO (Xue et al., 2025)	DPO	pLDDT score, designability	General protein sequences
	Park et al. (Park et al., 2024)	DPO	TM-score, diversity metric	Peptide / short-protein sequences
	RL-DIF (Ektefaie et al., 2024)	DDPO	Foldability, TM-score	General protein sequences
	ProtInvTree (Liu et al., 2025b)	MCTS	TM-score, scTM-score from ESMFold	General protein sequences
	DRAKES (Wang et al.)	Reward Fine-tuning	Sequence stability	General protein sequences
	GLID ² E (Cao et al., 2025a)	PPO	Sequence stability	General protein sequences
Antibody Engineering	AB-Gen (Xu et al., 2023b)	REINVENT	Developability, specificity	Antibody CDRH3 libraries (HER2, etc.)
	BetterBodies (Vogt et al., 2024)	Q-learning	Absolute free-energy, affinity	Antibody CDRH3 binders (SARS-CoV-2 RBD, etc.)
	Structured Q-learning (Cowen-Rivers et al., 2022)	Q-learning	Docking affinity	Antibody CDRH3 binders (IGG4, etc.)
Peptide Binder Design	TCRPPPO (Chen et al., 2023)	PPO	Valid-TCR likelihood, peptide-recognition probability	T-cell receptor (TCR) sequences (β -chain CDR3, etc.)
	HighPlay (Lin et al., 2025)	MCTS	Structure-/pose-guided scores, binding/energy proxies by HighFold	Cyclic peptide binders
	CYC_BUILDER MCTS (Wang et al., 2025a)		Docking/binding-energy, pose-quality scores	Cyclic peptide binders